

Interactions between particles with an undulated contact line at a fluid interface: Capillary multipoles of arbitrary order

Krassimir D. Danov^a, Peter A. Kralchevsky^{a,*}, Boris N. Naydenov^{a,1}, Günter Brenn^b

^a *Laboratory of Chemical Physics and Engineering, Faculty of Chemistry, University of Sofia, 1164 Sofia, Bulgaria*

^b *Institute of Fluid Mechanics and Heat Transfer, Graz University of Technology, 8010 Graz, Austria*

Received 19 September 2004; accepted 24 January 2005

Available online 5 March 2005

Abstract

A colloidal particle adsorbed at a fluid interface could have an undulated, or irregular contact line in the presence of surface roughness and/or chemical inhomogeneity. The contact-line undulations produce distortions in the surrounding liquid interface, whose overlap engenders capillary interaction between the particles. The convex and concave local deviations of the meniscus shape from planarity can be formally treated as positive and negative “capillary charges,” which form “capillary multipoles.” Here, we derive theoretical expressions for the interaction between two capillary multipoles of arbitrary order. Depending on the angle of mutual orientation, the interaction energy could exhibit a minimum, or it could represent a monotonic attraction. For undulation amplitudes larger than 5 nm, the interaction energy is typically much greater than the thermal energy kT . As a consequence, a monolayer from capillary multipoles exhibits considerable shear elasticity, and such monolayer is expected to behave as a two-dimensional elastic solid. These theoretical results could be helpful for the understanding of phenomena related to aggregation and ordering of particles adsorbed at a fluid interface, and for the interpretation of rheological properties of particulate monolayers. Related research fields are the particle-stabilized (Pickering) emulsions and the two-dimensional self-assembly of microscopic particles.

© 2005 Elsevier Inc. All rights reserved.

Keywords: Capillary force between particles; Capillary multipoles; Colloid particles—self-assembly; Interfacial rheology; Particles at interfaces; Particulate monolayers; Pickering emulsions; Surface shear elasticity

1. Introduction

The lateral capillary forces between particles, which are adsorbed at a fluid interface, have been found to play an important role in the creation of two-dimensional (2D) arrays of particles and proteins [1–5], the rheology of particulate monolayers [6,7], Pickering emulsions [8], development of coatings [9,10], new materials [11–16]. When the adsorbed particles have an undulated (or irregular) contact line, by analogy with electrostatics, the respective capillary force can be formally treated as interaction between 2D multipoles.

So far, only the charge–charge (monopole–monopole) and quadrupole–quadrupole capillary interaction have been theoretically investigated [5,17–20]. Here, our aim is to generalize the theory of this type of capillary interaction for multipoles of arbitrary order, including monopole–multipole. We first give a brief overview of previous results.

The origin of the lateral capillary forces is the overlap of perturbations in the shape of a liquid interface, which are produced by attached particles [17–19]; for reviews see Refs. [5,7,22]. In the case of floating heavy particles, the interfacial perturbations are caused by the particle weight (Fig. 1a). In this case, using the superposition approximation, one can derive the expression for the energy of capillary interaction between the two particles [7,18,19,22]

$$\Delta W = -2\pi\sigma Q_1 Q_2 K_0(qL), \quad (1.1)$$

* Corresponding author.

E-mail address: pk@lcepe.uni-sofia.bg (P.A. Kralchevsky).

¹ Current address: Department of Physics, Freie Universität, D-14195 Berlin, Germany.

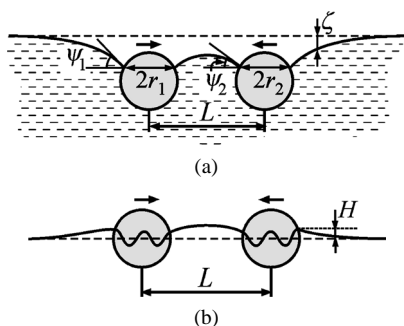


Fig. 1. Lateral capillary forces between floating particles: the interaction is due to the overlap of interfacial deformations created by the separate particles. (a) The deformations are caused by the action of a normal force: particle weight and buoyancy [18,19], or electro-dipping force [23,25]. (b) Even when the normal force is negligible, interfacial deformations could be engendered by an undulated contact line at the particle surface [6,7]. In this case, forces between the particles can be described as interactions between “capillary multipoles,” in analogy with electrostatics; see Eq. (1.6) [5,20,21].

where σ is the interfacial tension, L is the distance between the centers of the two particles; $Q_i = r_i \sin(\psi_i)$, $i = 1, 2$, are the so-called “capillary charges” [19]; r_i and ψ_i are the contact-line radius and the slope angle at the contact line of the respective particle, see Fig. 1a; and K_0 is the modified Bessel function of the second kind and zero order,

$$q^2 = \Delta\rho g / \sigma, \quad \Delta\rho = \rho_I - \rho_{II}, \quad (1.2)$$

where g is the acceleration due to gravity and ρ_I and ρ_{II} are the mass densities of the lower and upper fluid phases. For a floating spherical particle, the capillary charge is given by the expression [7,18,19]

$$Q_i \approx \frac{1}{6} q^2 R_i^3 (2 - 4D_i + 3 \cos \alpha_i - \cos^3 \alpha_i) \quad (i = 1, 2), \quad (1.3)$$

where R_i and α_i ($i = 1, 2$) are the particle radius and contact angle; $D_i = (\rho_i - \rho_{II}) / (\rho_I - \rho_{II})$; and ρ_i is the particle mass density. Equation (1.3) is valid for $qR_i \ll 1$. With the help of Eqs. (1.1)–(1.3) and typical parameter values, one can estimate that for $R_i < 5\text{--}10 \mu\text{m}$ the energy ΔW is smaller than the thermal energy kT , where k and T are the Boltzmann constant and absolute temperature. In other words, the capillary interaction between the particles becomes negligible. Physically, this means that in the case considered the particle weight is rather small to create significant interfacial deformation. Nevertheless, in the latter case, interfacial deformation could be created, but owing to an electric (electro-dipping) force, engendered by charges at the particle surface, rather than by the gravity effect [23–25].

Even in the absence of electro-dipping force, interfacial deformations can appear around small particles, if the contact line on the particle surface is undulated, as in Fig. 1b [5–7,20,21]. For example, this could happen in cases of angular or irregular particle shape, presence of surface roughness, chemical inhomogeneity, etc. The undulations of the contact line produce distortions in the surrounding liquid

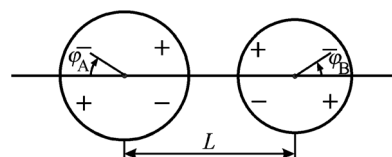


Fig. 2. Sketch of two particles, “capillary quadrupoles,” A and B, separated at a distance L . The signs “+” and “−” symbolize convex and concave local deviations of the contact line from planarity. The φ_A and φ_B denote the angles of rotation of the respective particles with respect to their initial state ($\varphi_A = \varphi_B = 0$).

interface, whose overlap also brings about a capillary interaction between the two particles. The interest toward such interactions has been growing during the last decade. First, Lucassen [6] investigated theoretically the capillary force between two cubic floating particles. He derived expression for the interaction energy per unit length of a contact line, which exhibits sinusoidal undulations in a vertical plane. The calculated capillary force has a minimum when the two particles are shifted normally or tangentially with respect to the contact line. As a consequence, the particulate monolayer exhibits elastic response to surface dilatational and shear deformations [6,7,21].

Stamou et al. [20] examined theoretically the case of spherical particles of undulated contact lines and derived an asymptotic expression for the interaction energy between two capillary quadrupoles,

$$\Delta W(L) \approx -12\pi\sigma H^2 \cos(2\varphi_A - 2\varphi_B) \frac{r_c^4}{L^4} \quad (L \gg 2r_c), \quad (1.4)$$

where H is amplitude of the undulation of the contact line, whose average radius is r_c ; the angles φ_A and φ_B are subtended between the diagonals of the respective quadrupoles and the line connecting the centers of the two particles (Fig. 2). The two particles spontaneously rotate to reach an optimal orientation for which the cosine in Eq. (1.4) is equal to one (maximal attraction and minimal energy). For example, taking $\sigma = 70 \text{ mN/m}$, $H = 20 \text{ nm}$, $r_c/L = 0.3$, from Eq. (1.4) we calculate $\Delta W = 2085kT$. In other words, we are dealing with a physically considerable effect.

In the case of two capillary quadrupoles, a more general expression for $\Delta W(L)$, valid in the whole range $2r_c \leq L < \infty$, has been derived in Ref. [21]. This expression predicts that an adsorption monolayer of particles, which behave as capillary quadrupoles, should exhibit considerable shear elasticity. In general, at close contact between such two particles, one could have $\Delta W \gg kT$ even for nm-sized particles [5,21]. This strong capillary interaction can cause a two-dimensional aggregation and ordering of sub- μm particles which are captive at a fluid interface. Multibody interactions between capillary quadrupoles have been investigated by Fournier and Galatola [26] who showed that a system, composed of a large number of such particles behaves as a jammed system.

Experimentally, interactions between capillary quadrupoles have been examined by Brown et al. [27], with photo-

lithography-fabricated curved discs, having one hydrophilic and one hydrophobic side. The contact line is attached to the edge of the curved disc. Different two-dimensional packing structures were obtained [27]. A variety of structures were produced in the experiments by Bowden and co-workers [2–4] on mesoscale self-assembly. Loudet et al. [28] reported that micrometer-sized prolate ellipsoids, trapped at an oil–water interface, experience strong, anisotropic, and long-ranged attractive capillary interaction, which can be explained if the interfacial ellipsoids are described as capillary quadrupoles.

Theoretically, to describe the meniscus shape for the system depicted in Fig. 1b, one has to solve the linearized Laplace equation of capillarity for small meniscus slope, $|\nabla\zeta|^2 \ll 1$:

$$\nabla^2\zeta = q^2\zeta. \quad (1.5)$$

Here ∇ is the two-dimensional gradient operator in the horizontal plane, xy . Using cylindrical coordinates (r, φ) , one can determine the interfacial shape, $z = \zeta(r, \varphi)$, around a single particle with an undulated contact line [5,20,21],

$$\zeta(r, \varphi) = A_0 K_0(qr) + \sum_{m=1}^{\infty} A_m K_m(qr) \cos[m(\varphi - \varphi_{0,m})], \quad (1.6)$$

were A_m and $\varphi_{0,m}$ are constants of integration, and K_m is the modified Bessel function of the second kind and m th order. Equation (1.6) can be considered as a multipole expansion (a two-dimensional analogue of that in electrostatics). The terms with $m = 0, 1, 2, 3, \dots$ correspond to “charge,” “dipole,” “quadrupole,” “hexapole,” etc.

Stamou et al. [20] noted that if the particles are freely floating, then the capillary force will spontaneously rotate each particle around a horizontal axis to annihilate the capillary dipole moment (unless the particle rotation is hindered); see Fig. 3. Therefore, the term with $m = 1$ in Eq. (1.6) has to be skipped. If the particles are sufficiently light, and the electro-dipping force [25] is negligible, then the zero-order term (the capillary charge) disappears, and the quadrupolar term (with $m = 2$) becomes the leading term in the multipole expansion, Eq. (1.6).

As already mentioned, for multipoles the sign and magnitude of the capillary force depend on the particle mutual

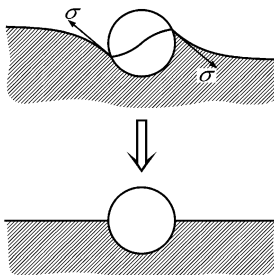


Fig. 3. The capillary force, due to the interfacial tension, σ , spontaneously rotates a freely floating particle to annihilate its capillary dipole moment ($m = 1$).

orientation. For that reason, particles–quadrupoles ($m = 2$) will tend to assemble in a square lattice, whereas particles–hexapoles ($m = 3$) will preferably form a hexagonal lattice, with or without voids (Fig. 4) [3–5]. Another possibility is that the particles could form simple linear (chain) aggregates [5,20]. Such structures have been observed experimentally [2–4,27].

As noted in the beginning, theoretical description is available for the case of interaction between two capillary charges [18,19] and two capillary quadrupoles [20,21]. In other words, the theoretical description is incomplete, because the forces between other types of capillary multipoles could be also of interest. For that reason, in the present paper we address the general problem for the interaction between two capillary multipoles, A and B, of arbitrary orders, m_A and m_B ($m_A, m_B = 0, 1, 2, 3, \dots$). For generality, we include the dipoles ($m_A, m_B = 1$), which could be realized at some special experimental conditions. (Dipolar interactions of nonelectric origin have been found to play an important role in various physical processes [29,30].)

In Section 2 we first consider an integral expression for the capillary interaction energy, $\Delta W(L)$, and other basic equations. Next, in Section 3 we determine the meniscus shape around two floating particles of undulated contact line by solving the Laplace equation of capillarity in bipolar coordinates. In Section 4 we derive an analytical expression for $\Delta W(L)$ in the general case $m_A, m_B \geq 2$ and $2r_c \leq L < \infty$. Numerical results for $\Delta W(L)$ are presented in the case of two capillary hexapoles. Convenient asymptotic equations are also derived. Section 5 is devoted to the interaction of a capillary charge ($m_A = 0$) with a higher order capillary multipole ($m_B \geq 1$). Finally, as an application, in Section 6 an expression is derived for the surface shear elasticity of an adsorption monolayer from identical capillary hexapoles.

2. Basic equations

We consider two solid particles, A and B, which are attached to a fluid–liquid interface that would be planar in the absence of particles. The horizontal projections of the contact lines at the particle surfaces are assumed to be circumferences, C_A and C_B , of radii r_A and r_B , respectively. We assume that the contact lines are undulated in a vertical direction,

$$\begin{aligned} \zeta_A &= H_A \cos[m_A(\varphi - \varphi_A)], \\ \zeta_B &= H_B \cos[m_B(\varphi - \varphi_B)], \end{aligned} \quad (2.1)$$

where H_A and H_B are the undulation amplitudes; m_A and m_B are the respective multipole orders ($m_A, m_B = 1, 2, 3, \dots$); φ is the running azimuthal angle, which provides parameterization of the respective circumference, C_A or C_B ; and the angles φ_A and φ_B characterize the rotation of the respective particles around a vertical axis (see Fig. 5).

The meniscus shape around such a particle in isolation can be found by solving the Laplace equation, Eq. (1.5), us-

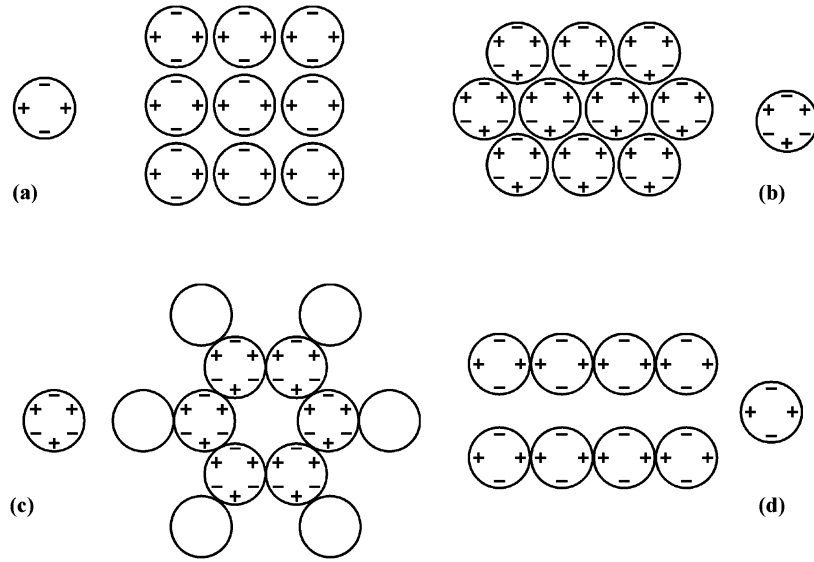


Fig. 4. 2D arrays formed by capillary quadrupoles ($m = 2$) and hexapoles ($m = 3$); the signs “+” and “-” denote, respectively, positive and negative “capillary charges,” i.e., convex and concave local deviations of the meniscus shape from planarity at the contact line. (a) Quadrupoles form tetragonal close-packed array [21,27]. Hexapoles could form (b) close-packed array; (c) hexagonal array with voids [2–4]. (d) Linear aggregates made of quadrupoles [20,27]. In contrast with the electric charges, two similar capillary charges attract each other, while the interaction between opposite capillary charges is repulsive.

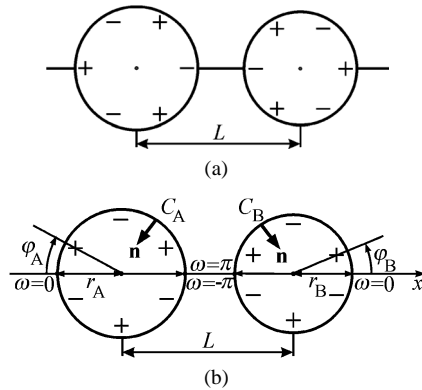


Fig. 5. Sketch of two “capillary hexapoles,” A and B, separated at a distance L . (a) Initial state. (b) An arbitrary mutual orientation characterized by the angles φ_A and φ_B ; C_A and C_B denote the projections of the respective contact lines, of radii r_A and r_B , on the xy -plane; \mathbf{n} is inner running unit normal to C_A and C_B . The angle ω of the bipolar coordinates varies in opposite directions along C_A and C_B .

ing Eq. (2.1) as a boundary condition. Thus, we obtain a special case of Eq. (1.6):

$$\zeta_Y(r, \varphi) = H_Y \frac{K_{m_Y}(qr)}{K_{m_Y}(qr_Y)} \cos[m_Y(\varphi - \varphi_Y)], \quad Y = A, B. \quad (2.2)$$

For the air–water interface, we have $q^{-1} = 2.7$ mm. On the other hand, our typical particle sizes and interparticle distances are much smaller. Then, for $qr \ll 1$, we can use the asymptotic form of the modified Bessel function: $K_m(x) \approx 1/x^m$ [31,32]. Correspondingly, Eq. (2.2) acquires the simpler form

$$\zeta_Y = H_B \frac{r_Y^{m_Y}}{r^{m_Y}} \cos[m_Y(\varphi - \varphi_Y)], \quad Y = A, B. \quad (2.3)$$

The meniscus excess surface energy, due to the deformation $z = \zeta(x, y)$, is equal to the product of the surface tension, σ , and the excess surface area [19,20],

$$W(L) = \sigma \int_{S_m} ds [(1 + |\nabla \zeta|^2)^{1/2} - 1] \approx \frac{\sigma}{2} \int_{S_m} ds |\nabla \zeta|^2, \quad (2.4)$$

where σ is the interfacial tension, S_m is the orthogonal projection of the meniscus on the xy -plane, and ds is the surface element.

In the limiting case of two noninteracting particles, A and B, which are separated at a long distance, $L \gg r_A, r_B$, $W(L)$ can be obtained by calculating the integral in Eq. (2.4) separately for ζ_A and ζ_B and summing the results. The differentiation of Eq. (2.3) yields

$$|\nabla \zeta_Y|^2 = m_Y^2 H_Y^2 \frac{r_Y^{2m_Y}}{r^{2m_Y+2}}. \quad (2.5)$$

Furthermore, we have

$$\int_{S_Y} |\nabla \zeta_Y|^2 ds = 2\pi m_Y^2 H_Y^2 r_Y^{2m_Y} \int_{r_Y}^{\infty} \frac{1}{r^{2m_Y+1}} dr = \pi m_Y H_Y^2 \quad (2.6)$$

($m_Y \geq 1$). Combining Eqs. (2.4) and (2.6), we obtain the meniscus excess surface energy in the limiting case $L \rightarrow \infty$:

$$W(\infty) = \frac{\pi \sigma}{2} (m_A H_A^2 + m_B H_B^2). \quad (2.7)$$

In the special case of $m_A = m_B = 2$, Eq. (2.7) reduces to the expression for capillary quadrupoles, derived in Ref. [20].

Now, let us return to the more general case, when the interfacial deformations around the two particles overlap. As discussed after Eq. (2.2), we are dealing with the case $qr \ll 1$, in which Eq. (1.5) can be written in a simpler form:

$$\nabla^2 \zeta = 0. \quad (2.8)$$

Note that Eq. (2.3) satisfies Eq. (2.8). Next, we make the transformation:

$$\nabla \cdot (\zeta \nabla \zeta) = (\nabla \zeta) \cdot \nabla \zeta + \zeta \nabla^2 \zeta = |\nabla \zeta|^2, \quad (2.9)$$

where at the last step we have used Eq. (2.8). Further, we combine Eqs. (2.4) and (2.9) and apply the Green theorem [33],

$$\begin{aligned} W(L) &= \frac{\sigma}{2} \int_{S_m} ds \nabla \cdot (\zeta \nabla \zeta) \\ &= \frac{\sigma}{2} \sum_{Y=A,B} \oint_{C_Y} dl \mathbf{n} \cdot (\zeta \nabla \zeta), \end{aligned} \quad (2.10)$$

where dl is the linear element along the contours C_A and C_B (Fig. 5b) and \mathbf{n} is an inner unit normal to the respective contour. Finally, the energy of capillary interaction is

$$\Delta W(L) = W(L) - W(\infty), \quad (2.11)$$

where $W(L)$ and $W(\infty)$ are given by Eqs. (2.10) and (2.7), respectively.

3. Meniscus shape in bipolar coordinates

3.1. Introduction of bipolar coordinates

To obtain explicit expressions for the meniscus shape, $\zeta(x, y)$, and the capillary interaction energy, $\Delta W(L)$, we will use bipolar coordinates in the xy -plane, which correspond to the geometry of the system; see, e.g., Refs. [34,35]. These coordinates, denoted τ and ω , are defined through the following set of equations:

$$\begin{aligned} x &= \chi \sinh(\tau), & y &= \chi \sin(\omega), \\ \chi &= a / (\cosh(\tau) - \cos(\omega)). \end{aligned} \quad (3.1)$$

The lines $\tau = \text{const.}$ and $\omega = \text{const.}$ are two families of mutually orthogonal circumferences (Fig. 6). In Eq. (3.1), a is a parameter related to the radii of the two contact lines, r_A and r_B , and to the distance between the two particles, L :

$$a^2 = \frac{1}{4L^2} [L^2 - (r_A + r_B)^2][L^2 - (r_A - r_B)^2]. \quad (3.2)$$

The projections of the two contact lines on the xy -plane, C_A and C_B , correspond to $\tau = -\tau_A$ and $\tau = \tau_B$, respectively, where

$$\tau_A = \text{arccosh} \left(\frac{L^2 + r_A^2 - r_B^2}{2Lr_A} \right),$$

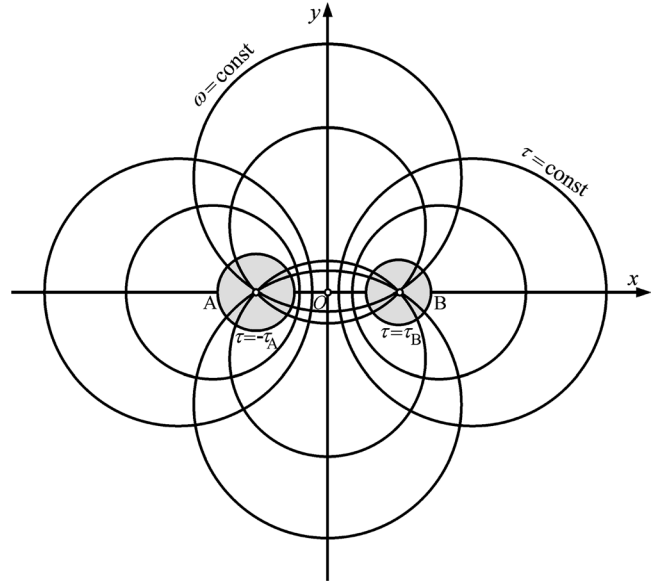


Fig. 6. Bipolar coordinates (τ, ω) in the xy -plane. The coordinate lines $\tau = \text{const.}$ and $\omega = \text{const.}$ represent two families of mutually orthogonal circumferences. The contact line projections, C_A and C_B , correspond to $\tau = -\tau_A$ and $\tau = \tau_B$.

$$\tau_B = \text{arccosh} \left(\frac{L^2 + r_B^2 - r_A^2}{2Lr_B} \right), \quad (3.3)$$

$$\text{arccosh}(x) = \ln[x + (x^2 - 1)^{1/2}]. \quad (3.4)$$

Other useful relationships, which follow from Eqs. (3.2) and (3.3), are

$$\sinh(\tau_A) = \frac{a}{r_A}, \quad \sinh(\tau_B) = \frac{a}{r_B}. \quad (3.5)$$

In bipolar coordinates, the linearized Laplace equation of capillarity, Eq. (2.8), acquires the form

$$\frac{\partial^2 \zeta}{\partial \tau^2} + \frac{\partial^2 \zeta}{\partial \omega^2} = 0, \quad (3.6)$$

where $\zeta = \zeta(\tau, \omega)$, is the deviation of the fluid interface from planarity. We will seek the solution of Eq. (3.6) in the form of a Fourier expansion:

$$\begin{aligned} \zeta &= H_B \sum_{n=1}^{\infty} [C_n \cos(n\omega) + D_n \sin(n\omega)] \frac{\sinh[n(\tau_A + \tau)]}{\sinh[n(\tau_A + \tau_B)]} \\ &\quad + H_A \sum_{n=1}^{\infty} [E_n \cos(n\omega) + F_n \sin(n\omega)] \frac{\sinh[n(\tau_B - \tau)]}{\sinh[n(\tau_A + \tau_B)]}. \end{aligned} \quad (3.7)$$

3.2. Determination of the unknown coefficients

To determine the unknown coefficients, C_n , D_n , E_n , and F_n , we substitute Eq. (3.7) in the boundary condition, Eq. (2.1). Thus we obtain

$$\begin{aligned} \cos[m_B(\varphi - \varphi_B)] &= \sum_{n=1}^{\infty} [C_n \cos(n\omega) + D_n \sin(n\omega)] \\ &\text{at } \tau = \tau_B, \end{aligned} \quad (3.8)$$

$$\cos[m_A(\varphi - \varphi_A)] = \sum_{n=1}^{\infty} [E_n \cos(n\omega) + F_n \sin(n\omega)]$$

at $\tau = -\tau_A$. (3.9)

To proceed further, we need a connection between the angles φ and ω . For simplicity, we choose the direction of increase of angle φ to be the same as of ω , that is clockwise for the circumference C_A , and anticlockwise for C_B . Next, in the relationship $\sin(\varphi) = y/r_Y$, we substitute y from Eq. (3.1) and r_Y from Eq. (3.5); thus, we obtain

$$\sin(\varphi) = \frac{\sinh(\tau_Y) \sin(\omega)}{\cosh(\tau_Y) - \cos(\omega)} \quad (Y = A, B). \quad (3.10)$$

From Eq. (3.10) we deduce [35]

$$\cos(\varphi) = \frac{\cosh(\tau_Y) \cos(\omega) - 1}{\cosh(\tau_Y) - \cos(\omega)} \quad (Y = A, B). \quad (3.11)$$

Equations (3.10) and (3.11) indicate that $\sin(\varphi)$ and $\cos(\varphi)$ are, respectively, odd and even functions of ω . Hence, we have

$$\int_{-\pi}^{\pi} \cos(m\varphi) \sin(n\omega) d\omega = 0,$$

$$\int_{-\pi}^{\pi} \sin(m\varphi) \cos(n\omega) d\omega = 0. \quad (3.12)$$

With the help of Eq. (3.12), from Eqs. (3.8) and (3.9) we derive

$$C_n = \cos(m_B \varphi_B) A(n, m_B, \tau_B),$$

$$D_n = \sin(m_B \varphi_B) B(n, m_B, \tau_B), \quad (3.13)$$

$$E_n = \cos(m_A \varphi_A) A(n, m_A, \tau_A),$$

$$F_n = \sin(m_A \varphi_A) B(n, m_A, \tau_A), \quad (3.14)$$

where the functions $A(n, m, \tau_Y)$ and $B(n, m, \tau_Y)$ do not depend on the angles φ_A and φ_B , and are defined as

$$A(n, m, \tau_Y) = \frac{1}{\pi} \int_{-\pi}^{\pi} \cos(m\varphi) \cos(n\omega) d\omega, \quad (3.15)$$

$$B(n, m, \tau_Y) = \frac{1}{\pi} \int_{-\pi}^{\pi} \sin(m\varphi) \sin(n\omega) d\omega, \quad (3.16)$$

where φ is related to ω by means of Eq. (3.10). In Appendix A, we prove that

$$A(n, m, \tau_Y) = B(n, m, \tau_Y)$$

$$= \frac{1}{(m-1)!} \frac{d^{m-1}}{dz^{m-1}} [z^{n-1} (1 - \beta z)^m] \Big|_{z=\beta}, \quad (3.17)$$

$$\beta = \exp(-\tau_Y) \quad (Y = A, B). \quad (3.18)$$

For computations, it is more convenient to carry out the differentiation in Eq. (3.17) and to present the result as a

polynomial (see Appendix A),

$$A(n, m, \tau_Y) = m \sum_{k=0}^{\min(m,n)} \frac{(-1)^{m-k} (m+n-k-1)!}{(m-k)!(n-k)!k!} \beta^{m+n-2k}, \quad (3.19)$$

where $\min(m, n)$ denotes the smallest of m and n . Finally, in view of Eqs. (3.13), (3.14), and (3.17), Eq. (3.7) acquires the form

$$\zeta = H_A \sum_{n=1}^{\infty} A(n, m_A, \tau_A) \cos(n\omega - m_A \varphi_A)$$

$$\times \frac{\sinh[n(\tau_B - \tau)]}{\sinh[n(\tau_A + \tau_B)]}$$

$$+ H_B \sum_{n=1}^{\infty} A(n, m_B, \tau_B) \cos(n\omega - m_B \varphi_B)$$

$$\times \frac{\sinh[n(\tau_A + \tau)]}{\sinh[n(\tau_A + \tau_B)]}, \quad (3.20)$$

where $A(n, m, \tau_Y)$ is given by Eq. (3.19).

4. Energy of interaction between multipoles

4.1. General expression

In bipolar coordinates, Eq. (2.10) takes the form

$$W(L) = \frac{\sigma}{2} \int_{-\pi}^{\pi} d\omega \zeta(\omega, \tau_B) \frac{\partial \zeta}{\partial \tau} \Big|_{\tau=\tau_B}$$

$$- \frac{\sigma}{2} \int_{-\pi}^{\pi} d\omega \zeta(\omega, -\tau_A) \frac{\partial \zeta}{\partial \tau} \Big|_{\tau=-\tau_A}. \quad (4.1)$$

Next, from Eq. (3.20) we calculate the derivative $\partial \zeta / \partial \tau$, which is then substituted into Eq. (4.1). The result can be obtained in a relatively compact form with the help of the identities

$$\int_{-\pi}^{\pi} \cos(k\omega - m_Y \varphi_Y) \cos(n\omega - m_Y \varphi_Y) d\omega = \pi \delta_{k,n}, \quad (4.2)$$

$$\int_{-\pi}^{\pi} \cos(k\omega - m_A \varphi_A) \cos(n\omega - m_B \varphi_B) d\omega$$

$$= \pi \cos(m_B \varphi_B - m_A \varphi_A) \delta_{k,n}. \quad (4.3)$$

Thus, we derive the sought-for expression for the surface excess energy $W(L)$,

$$\frac{W(L)}{\pi \sigma} = H_A^2 S_A + H_B^2 S_B - H_A H_B G \cos(m_B \varphi_B - m_A \varphi_A), \quad (4.4)$$

where

$$S_Y = \sum_{n=1}^{\infty} \frac{n}{2} \coth[n(\tau_A + \tau_B)] A^2(n, m_Y, \tau_Y) \quad (Y = A, B), \quad (4.5)$$

$$G \equiv \sum_{n=1}^{\infty} \frac{nA(n, m_A, \tau_A)A(n, m_B, \tau_B)}{\sinh[n(\tau_A + \tau_B)]}. \quad (4.6)$$

The energy of capillary interaction, $\Delta W(L)$, can be obtained by substitution of Eq. (4.4) into Eq. (2.11). This in principle, solves the problem, because $A(n, m, \tau_Y)$ is a known function, given by Eq. (3.19). The derivative, $F = -dW(L)/dL$, gives the interaction force. For $m_A = m_B = 2$, Eq. (4.4) reduces to Eq. (3.17) in Ref. [21]; note that (by definition) φ_A in the latter reference is $\pi - \varphi_A$ in the present paper.

In the case of close contact, $L \rightarrow r_A + r_B$, from Eqs. (3.2) and (3.5) we obtain $a = 0$ and $\tau_A = \tau_B = 0$. At a first glance, it could seem that S_Y and G , given by Eqs. (4.5) and (4.6), are divergent in this limit. However, it turns out that for $L \rightarrow r_A + r_B$, the functions S_Y and G take finite values, because the numerators in Eqs. (4.5) and (4.6) tend to zero. The respective limiting values of S_Y and G can be computed numerically.

Equations (4.4)–(4.6) are applicable to calculation of the interaction energy between two capillary multipoles for every $m_A, m_B \geq 1$, and for $r_A + r_B \leq L < \infty$. The condition $m_A, m_B \geq 1$ is necessary, because if $m_Y = 0$ (capillary charge), the integral in Eq. (2.6) is divergent. For this reason, in Section 5 we separately investigate the interaction of a capillary charge with capillary multipoles of various orders.

4.2. Asymptotics for large distance L

For large interparticle distances, we have

$$\beta_Y \equiv \exp(-\tau_Y) \approx \frac{r_Y}{L} \ll 1 \quad (Y = A, B); \quad (4.7)$$

see Eqs. (3.3) and (3.4). With the help of Eq. (4.7), one can determine the leading terms in the asymptotics of S_A , S_B , and G for large L , see Eqs. (4.5), (4.6) and Appendix B,

$$S_A = \frac{m_A}{2} + m_A^2 \frac{r_A^{2m_A}}{L^{2m_A}} \frac{r_B^2}{L^2} + \dots, \quad (4.8)$$

$$S_B = \frac{m_B}{2} + m_B^2 \frac{r_A^2}{L^2} \frac{r_B^{2m_B}}{L^{2m_B}} + \dots, \quad (4.9)$$

$$G = G_0 \frac{r_A^{m_A}}{L^{m_A}} \frac{r_B^{m_B}}{L^{m_B}} + \dots, \quad (4.10)$$

where G_0 is constant (independent of L):

$$G_0 = \sum_{n=1}^{\min(m_A, m_B)} \frac{2(-1)^{m_A+m_B} m_A! m_B!}{(m_A - n)! (m_B - n)! n! (n - 1)!}. \quad (4.11)$$

Values of G_0 corresponding to different m_A and m_B are listed in Table 1.

One can check that the first terms in Eqs. (4.8) and (4.9), $m_A/2$ and $m_B/2$, after substitution into Eq. (4.4), give the expression for $W(\infty)$, Eq. (2.7). Then, for $|m_A - m_B| \leq 1$, the leading term in ΔW for $L \rightarrow \infty$ comes from the function

Table 1
Values of G_0 for different m_A and m_B

m_A	m_B	G_0
2	2	12
2	3	-24
2	4	40
2	5	-60
3	3	60
3	4	-120
3	5	210
4	4	280
4	4	-560
5	5	1260

G , see Eqs. (2.11), (4.4), and (4.10):

$$\Delta W(L) \approx -\pi\sigma G_0 H_A H_B \cos(m_A \varphi_A - m_B \varphi_B) \frac{r_A^{m_A} r_B^{m_B}}{L^{(m_A+m_B)}}. \quad (4.12)$$

For two quadrupoles, $m_A = m_B = 2$, we have $G_0 = 12$, and Eq. (4.12) gives Eq. (1.4) as a special case for $H_A = H_B = H$ and $r_A = r_B = r_c$. For two hexapoles, $m_A = m_B = 3$, we have $G_0 = 60$, and Eq. (4.12) reduces to

$$\Delta W(L) \approx -60\pi\sigma H^2 \cos(3\varphi_A - 3\varphi_B) \frac{r_c^6}{L^6} \quad (L \gg 2r_c). \quad (4.12a)$$

If the particles are free to rotate around a vertical axis, the orientational angles φ_A and φ_B will spontaneously reach appropriate values, for which the cosine in Eq. (4.12) is equal to 1 for $G_0 > 0$ (or -1 for $G_0 < 0$), and thus to reach the minimal value of ΔW (the maximal attraction) for the given L .

In Table 2, we give the form of Eq. (4.12) for some special cases, corresponding to different m_A and m_B , including the case with $m_A = 0$, where one of the two interacting particles represents capillary charge. The latter case is investigated in Section 5.

4.3. Example: interaction between two hexapoles

To calculate the exact dependence $\Delta W(L)$, we used Eqs. (4.4)–(4.6), together with Eq. (3.3). Fig. 7 shows $\Delta W(L)$ curves for two identical particles–hexapoles: $H_A = H_B = H$ and $r_A = r_B = r_c$. The different curves correspond to different values of the phase angle,

$$\Delta\varphi \equiv 3\varphi_A - 3\varphi_B; \quad (4.13)$$

see Fig. 5b. For $5^\circ < \Delta\varphi < 25^\circ$, the dependence $\Delta W(L)$ has a minimum; i.e., the interaction is attractive at long distances and repulsive at short distances. In contrast, for $0 \leq \Delta\varphi < 5^\circ$ the interaction is attraction at all distances. This result qualitatively resembles the results for two capillary quadrupoles [21].

The global minimum of ΔW (maximal attraction), which corresponds to $\Delta\varphi = 0$ and $L = 2r_c$, is

$$\Delta W_{\min} \approx -0.6(\pi\sigma H^2). \quad (4.14)$$

Table 2
Asymptotic expressions for $\Delta W(L)$ for some values of m_A and m_B

Type of interaction	(m_A, m_B)	Interaction energy $\Delta W(L)$ for $r_A, r_B \ll L \ll q^{-1}$
Charge–quadrupole	(0, 2)	$-\frac{\pi}{2}\sigma Q_A H_B \cos[2(\varphi_B - \pi)]\left(\frac{r_B}{L}\right)^2$
Charge–multipole	(0, m_B)	$-\frac{\pi}{2}\sigma Q_A H_B \cos[m_B(\varphi_B - \pi)]\left(\frac{r_B}{L}\right)^{m_B}$
Dipole–quadrupole	(1, 2)	$4\pi\sigma H_A H_B \cos[\varphi_A - 2\varphi_B]\frac{r_A r_B^2}{L^3}$
Quadrupole–quadrupole	(2, 2)	$-12\pi\sigma H_A H_B \cos[2(\varphi_A - \varphi_B)]\frac{(r_A r_B)^2}{L^4}$
Quadrupole–hexapole	(2, 3)	$24\pi\sigma H_A H_B \cos(2\varphi_A - 3\varphi_B)\frac{r_A^2 r_B^3}{L^5}$
Hexapole–hexapole	(3, 3)	$-60\pi\sigma H_A H_B \cos(3\varphi_A - 3\varphi_B)\frac{r_A^3 r_B^3}{L^6}$
Hexapole–octupole	(3, 4)	$120\pi\sigma H_A H_B \cos(3\varphi_A - 4\varphi_B)\frac{r_A^3 r_B^4}{L^7}$
Multipole–multipole	(m_A, m_B)	$-G_0\pi\sigma H_A H_B \cos(m_A\varphi_A - m_B\varphi_B)\frac{r_A^{m_A} r_B^{m_B}}{L^{(m_A+m_B)}}$

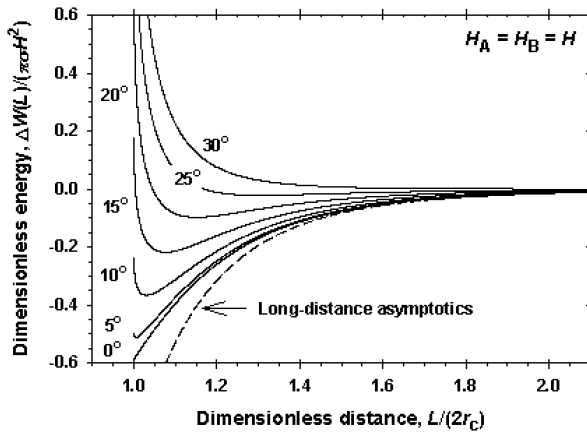


Fig. 7. Energy of interaction between two capillary hexapoles ($m_A = m_B = 3$), $\Delta W(L)$, scaled with $\pi\sigma H^2$, plotted vs $L/(2r_c)$. The lines are calculated by means of Eqs. (4.4)–(4.6) and (3.3) for two identical particles: $H_A = H_B = H$; $r_A = r_B = r_c$. The different curves correspond to different values of the phase angle $\Delta\varphi$, denoted in the figure. The dashed line represents the asymptotic expression for large interparticle distances, Eq. (4.12a), for $\Delta\varphi = 0$.

For $\sigma = 70$ mN/m, $H = 10$ nm, and $T = 25^\circ\text{C}$, from Eq. (4.14) we calculate $\Delta W_{\min} = -3218kT$. This result indicates again that the energy of this type of capillary interaction is very large compared to the thermal energy kT , even for undulations of amplitude 10 nm. It is worth noting that for a given H , ΔW_{\min} does not depend on r_c (that is on the particle size), see Eq. (4.14). In other words, for the same H , the energy of capillary attraction at close contact is the same for hexapoles of radius, say, 100 nm and 10 μm .

The lowest dashed line in Fig. 7 is calculated with the asymptotic formula, Eq. (4.12a), for $m_A = m_B = 3$ and $\Delta\varphi = 0$. In the figure it is seen that the asymptotic formula becomes sufficiently accurate for $L/(2r_c) > 1.5$. Note, however, that this asymptotic formula cannot describe the non-monotonic behavior of $\Delta W(L)$ for $5^\circ < \Delta\varphi < 25^\circ$.

Due to the cosine in Eq. (4.4), at fixed L , the function $\Delta W(\Delta\varphi)$ has a pronounced minimum at $\Delta\varphi = 0$. As in the case of capillary quadrupoles [21], the existence of such a minimum is the reason for the appearance of consider-

able shear elasticity in adsorption monolayers of particles–hexapoles. Expression for the respective modulus of shear elasticity is derived in Section 6.

5. Interaction between a capillary charge and a capillary multipole

5.1. Meniscus profile

We consider again two solid particles, A and B, which are attached to a fluid–liquid interface. The horizontal projections of the contact lines at the particle surfaces are assumed to be circumferences, C_A and C_B , of radii r_A and r_B , respectively. We assume that particle A is a capillary charge, while particle B is a capillary multipole of order m_B ($m_B = 1, 2, 3, \dots$). As before, the meniscus shape is described by the equation $z = \zeta(x, y)$. At the contact lines we have the following boundary conditions:

$$\zeta|_{C_A} = H_A, \quad \zeta|_{C_B} = H_B \cos[m_B(\varphi - \varphi_B)]. \quad (5.1)$$

To solve the problem, in this section we use the superposition method; i.e., we try the solution in the form

$$\zeta = \zeta_A + \zeta_B, \quad (5.2)$$

where ζ_A and ζ_B satisfy the linearized Laplace equation of capillarity,

$$\nabla^2 \zeta_A = q^2 \zeta_A, \quad \nabla^2 \zeta_B = q^2 \zeta_B, \quad (5.3)$$

see Eq. (1.5), and the boundary conditions

$$\zeta_A|_{C_A} \equiv \zeta_{A,c} = H_A, \quad (5.4)$$

$$\zeta_B|_{C_B} \equiv \zeta_{B,c} = H_B \cos[m_B(\varphi - \varphi_B)], \quad (5.5)$$

$$\zeta_A|_{C_B} = \zeta_B|_{C_A} = 0. \quad (5.6)$$

The boundary conditions (5.4)–(5.6) guarantee the fulfillment of the boundary condition (5.1). In the case $qL \ll 1$, the solution for ζ_B , which satisfies Eqs. (5.5) and (5.6), can

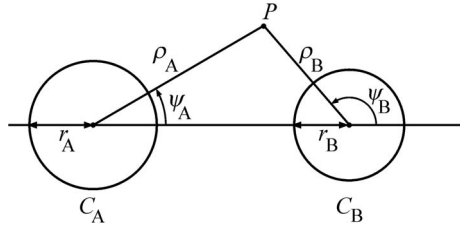


Fig. 8. Two sets of polar coordinates in the xy -plane, (ρ_A, ψ_A) and (ρ_B, ψ_B) , associated with the two particles. P is an arbitrary point in the plane. C_A and C_B are circumferences of radius r_A and r_B , respectively, representing the horizontal projections of the respective contact lines.

be determined by substituting $H_A = 0$ in Eq. (3.20):

$$\zeta_B = H_B \sum_{n=1}^{\infty} A(n, m_B, \tau_B) \cos(n\omega - m_B\varphi_B) \times \frac{\sinh[n(\tau_A + \tau)]}{\sinh[n(\tau_A + \tau_B)]}. \quad (5.7)$$

On the other hand, ζ_A can be presented in the form

$$\zeta_A = Q_A K_0(q\rho_A) + \zeta_A^{\text{corr}}, \quad H_A = Q_A K_0(qr_A), \quad (5.8)$$

where Q_A is the capillary charge, ρ_A is a position vector shown in Fig. 8, and ζ_A^{corr} is a small correction of the leading order solution. The role of ζ_A^{corr} , which also satisfies the Laplace equation (5.3), is to guarantee the fulfillment of the boundary condition (5.6):

$$\zeta_A^{\text{corr}}|_{C_A} = 0, \quad \zeta_A^{\text{corr}}|_{C_B} = -Q_A K_0(q\rho_A). \quad (5.9)$$

5.2. Interaction energy

In the considered case, $qL \ll 1$, we can use Eqs. (2.10) and (4.1) for the meniscus excess surface energy, $W(L)$. In view of the latter two equations, using Eqs. (5.4) and (5.7), one can present the integral over C_A in the form

$$\oint_{C_A} dl [\mathbf{n} \cdot \nabla(\zeta_A + \zeta_B)] \zeta_{A,c} = H_A \oint_{C_A} dl (\mathbf{n} \cdot \nabla \zeta_A). \quad (5.10)$$

Using the approach from Section 4.1, we express the integral over C_B in the form

$$\oint_{C_B} dl [\mathbf{n} \cdot \nabla(\zeta_A + \zeta_B)] \zeta_{B,c} = \oint_{C_B} dl (\mathbf{n} \cdot \nabla \zeta_A) \zeta_{B,c} + 2\pi H_B^2 S_B, \quad (5.11)$$

where Eqs. (5.5) and (5.7) have been used; S_B is defined by Eq. (5.5). Finally, from Eqs. (2.10), (5.2), (5.4)–(5.6), (5.10), and (5.11), we obtain

$$\frac{2}{\sigma} W(L) = H_A \oint_{C_A} dl (\mathbf{n} \cdot \nabla \zeta_A) + \oint_{C_B} dl (\mathbf{n} \cdot \nabla \zeta_A) \zeta_{B,c} + 2\pi H_B^2 S_B. \quad (5.12)$$

Let us first calculate the cross-interaction integral in Eq. (5.12), defined as

$$I_{AB} \equiv \oint_{C_B} dl (\mathbf{n} \cdot \nabla \zeta_A) \zeta_{B,c}. \quad (5.13)$$

In the calculations we will use two sets of polar coordinates in the xy -plane, (ρ_A, ψ_A) and (ρ_B, ψ_B) , with respect to the two particles (Fig. 8). A helpful relationship between these coordinates is given by the cosine theorem:

$$\rho_A^2 = L^2 + \rho_B^2 + 2L\rho_B \cos \psi_B. \quad (5.14)$$

In terms of these coordinates, we can express Eq. (5.13) in the form

$$I_{AB} = -H_B r_B \cos(m_B \varphi_B) \int_0^{2\pi} \cos(m_B \psi_B) \frac{\partial \zeta_A}{\partial \rho_B} d\psi_B, \quad (5.15)$$

where we have substituted $\zeta_{B,c}$ from Eq. (5.5) and have used that ζ_A is an even function of ψ_B . Further, with the help of Eqs. (5.8) and (5.14), we calculate the derivative in Eq. (5.15) up to terms on the order of $(qL)^2$:

$$\frac{\partial \zeta_A}{\partial \rho_B} = Q_A \frac{dK_0(q\rho_A)}{d\rho_A} \frac{\partial \rho_A}{\partial \rho_B} = -\frac{Q_A}{\rho_A^2} (\rho_B + L \cos \psi_B). \quad (5.16)$$

With $\rho_B = r_B$ and ρ_A given by Eq. (5.14), we substitute Eq. (5.16) into Eq. (5.15) and carry out the integration. The result reads

$$I_{AB} = -\pi Q_A H_B \cos[m_B(\varphi_B - \pi)] \frac{r_B^{m_B}}{L^{m_B}}. \quad (5.17)$$

Further, using Eq. (5.8), we obtain

$$\oint_{C_A} dl (\mathbf{n} \cdot \nabla \zeta_A) = 2\pi Q_A + I_{AA}, \quad (5.18)$$

where

$$I_{AA} = \oint_{C_A} dl (\mathbf{n} \cdot \nabla \zeta_A^{\text{corr}}). \quad (5.19)$$

With the help of Eq. (5.14), in the boundary condition at C_B , Eq. (5.9), we expand in series for $qL \ll 1$ and $r_B/L \ll 1$:

$$\frac{\zeta_A^{\text{corr}}}{Q_A} = -K_0(qL) + \frac{r_B}{L} \cos \psi_B - \frac{1}{2} \left(\frac{r_B}{L} \right)^2 \cos(2\psi_B) + \dots \quad \text{at } C_B. \quad (5.20)$$

Using Eq. (5.20), we obtain ζ_A^{corr} as a solution of the Laplace equation (5.3), in a form analogous to the multipole expansion, Eq. (1.6):

$$\zeta_A^{\text{corr}} = -Q_A \frac{K_0(qL)}{K_0(qr_B)} K_0(q\rho_B) + Q_A \frac{r_B}{L} \frac{r_B}{\rho_B} \cos \psi_B + \dots \quad (5.21)$$

One could check that the substitution of Eq. (5.21) into Eq. (5.19) yields $I_{AA} = 0$, within an accuracy $O[(r_B/L)^5]$.

Using Eqs. (5.10), (5.11), (5.13), (5.17), and (5.18), we can rewrite Eq. (5.12) in the form

$$\frac{W(L)}{\pi\sigma} = Q_A^2 G_A + H_B^2 S_B - \frac{1}{2} Q_A H_B \cos[m_B(\varphi_B - \pi)] \frac{r_B^{m_B}}{L^{m_B}}, \quad (5.22)$$

where $G_A = K_0(qr_A) + O[(r_Y/L)^5]$; see Eq. (5.8).

5.3. Discussion

In fact, the last term in Eqs. (4.4) and (5.22), which depends on the angles of mutual orientation, φ_A and φ_B , give the essential part of the interaction between the two capillary multipoles. The other terms, proportional to $S_A(L)$, $S_B(L)$, and $G_A(L)$, originate from the “rigid” boundary conditions imposed at the contact lines; see, e.g., Eqs. (5.4)–(5.6). For example, the requirement $\zeta_A|_{C_B} = 0$ leads to the appearance of a series of correction multipole expansion at C_B ; see Eq. (5.20). However, if the particle B is freely floating, then the mean level and slope of its contact line will adjust to comply with the mean elevation and slope of $\zeta_A(\rho_A)$ at C_B . To take into account such effects of “contact-line adjustment,” one has to carry out additional theoretical investigation, which is out of the scope of the present article.

6. Shear elasticity of monolayer from hexapoles

6.1. Basic equations

Here, we give an application of the derived equations to derive an expression for the shear elasticity of a monolayer of particles, which behave as capillary hexapoles. Such particles have been investigated experimentally [2–4]. Our results represent an upgrade of Ref. [21], where analogous expressions for capillary quadrupoles have been derived.

We consider an adsorption layer of capillary hexapoles, which is subjected to shear along the y -axis; see Fig. 9. Following the thermodynamic approach of Landau and Lifshitz [36], one can determine the shear elastic modulus, E_S , by differentiation of the free energy of the system, Ω , with respect to the shear deformation (see Eq. (4.1) in Ref. [36]),

$$E_S = \frac{1}{2u_{yx}} \frac{\partial \Omega}{\partial u_{yx}}, \quad (6.1)$$

where the coefficient of surface shear elasticity, E_S , is a 2D analogue of the coefficient of Lamé, μ , in Ref. [36]. Ω is free energy (or grand thermodynamic potential) per unit area of the adsorption layer. For small shear angles, the relative displacement along the y -axis, $u_{yx} = (\partial u_y / \partial x)/2$, is equal to $\varphi_S/2$, where φ_S is the shearing angle. For not-too-small particles, the entropy contribution in Ω is small in comparison with the contribution from the particle–particle interaction energy. Then an approximate expression for Ω can be obtained by taking into account only the interactions between

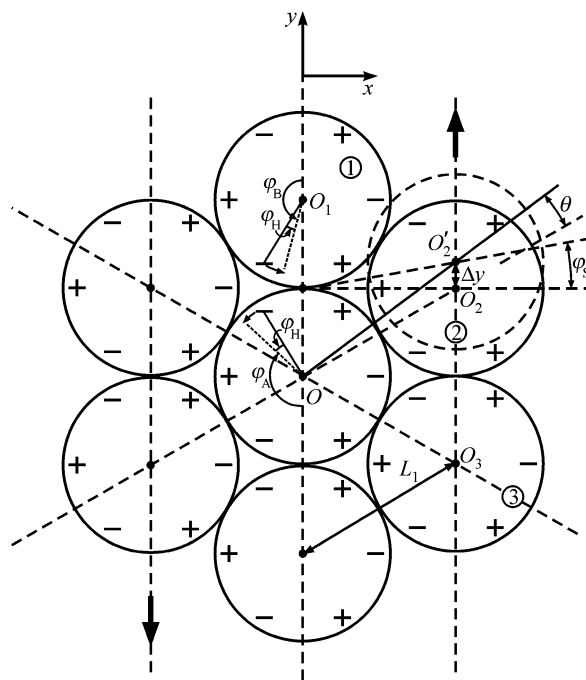


Fig. 9. Hexagonally packed layer of capillary hexapoles, which is subjected to shear deformation along the y -axis. L_1 is the center-to-center distance between two neighboring particles; φ_S is the shearing angle; φ_H is the angle of rotation of each particle due to the shear deformation; the other notations are explained in the text.

the first neighbors in the particle monolayer:

$$\Omega \approx \frac{1}{2} N_1 U(L_1) = \frac{U(L_1)}{\sqrt{3} L_1^2}. \quad (6.2)$$

Here, N_1 is the number of particles per unit area of the adsorption monolayer; L_1 is the distance between two neighboring particles (Fig. 9); and $U(L_1)$ is the interaction of a given particle in the monolayer with all of its first neighbors. The multiplier 1/2 in Eq. (6.2) appears because we must account only once for the interaction for each pair of particles. We have also used the fact that for hexagonal packing, the area per particle in the monolayer is $A_1 = 1/N_1 = (\sqrt{3}/2)L_1^2$. Having in mind that $u_{yx} = \varphi_S/2$, we combine Eqs. (6.1) and (6.2) to obtain

$$E_S = \frac{2}{\sqrt{3}} \frac{1}{L_1^2 \varphi_S} \frac{\partial U(L_1)}{\partial \varphi_S}. \quad (6.3)$$

During the shear deformation, depicted in Fig. 9, the neighboring “columns” of particles undergo mutual displacement along the y -axis. Thus, the right-hand side column is sifted at a distance Δy with respect to the central column (Fig. 9). The shear angle is

$$\varphi_S \approx \frac{\Delta y}{\Delta x} = \frac{\Delta y}{L_1 \sin(60^\circ)} = \frac{2\Delta y}{\sqrt{3}L_1}, \quad (6.4)$$

where Δx is the distance between the two columns. On the other hand, in the derivations below we will employ the aux-

iliary angle θ , which is defined as follows (see Fig. 9):

$$\theta \approx \frac{\Delta y \sin(60^\circ)}{L_1} = \frac{\sqrt{3}\Delta y}{2L_1}. \quad (6.5)$$

Comparing Eqs. (6.4) and (6.5), we obtain

$$\theta = \frac{3}{4}\varphi_S. \quad (6.6)$$

6.2. Interaction of a given particle with its first neighbors

The interaction energy, $U(L_1)$, of the central particle in Fig. 9 with its first neighbors can be expressed in the form

$$U = 2(W_1 + W_2 + W_3), \quad (6.7)$$

where W_1 , W_2 , and W_3 is the energy of interaction of the central particle, respectively, with particles 1, 2, and 3, shown in Fig. 9. The multiplier 2 in Eq. (6.7) accounts for the fact that the energy of interaction with the remaining three neighbors is the same as with the particles 1, 2, and 3, owing to the symmetry of the system. For identical capillary hexapoles, $m_A = m_B = 3$, Eq. (4.4) yields

$$W(L_1) = \pi\sigma H^2[2S_1 - G_1 \cos(3\varphi_B - 3\varphi_A)], \quad (6.8)$$

where

$$H = H_A = H_B, \quad S_1 = S_A(L_1) = S_B(L_1), \\ G_1 = G(L_1). \quad (6.9)$$

As noted in Ref. [21], the shear leads to a rotation of the hexapoles to a given angle (with respect to their initial orientation), which will be denoted by φ_H . In general, $\varphi_H \neq \varphi_S$. Since the particles have identical environment, it is natural to assume that the angle of rotation, φ_H , is the same for all of them. Following Ref. [21], we will find φ_H by minimization of the total interaction energy between the particles, $U(L_1, \varphi_S, \varphi_H)$:

$$\left. \frac{\partial U}{\partial \varphi_H} \right|_{\varphi_S, L_1} = 0. \quad (6.10)$$

First, let us consider the interaction of the ‘‘central particle’’ with ‘‘particle 1’’ (Fig. 9). Both particles are rotated at an angle φ_H , counterclockwise. If we take as reference mark the negative ‘‘capillary charge’’ denoted in Fig. 9, then for the central particle we have $\varphi_A = (5/6)\pi - \varphi_H$. In addition, for particle 1 we have $\varphi_B = (5/6)\pi + \varphi_H$. Consequently, $\Delta\varphi \equiv \varphi_B - \varphi_A = 2\varphi_H$. Substituting the latter value into Eq. (6.8), we get

$$W_1 = \pi\sigma H^2[2S_1 - G_1 \cos(6\varphi_H)]. \quad (6.11)$$

Second, let us consider the interaction of the central particle with particle 2 (Fig. 10). Taking as a reference marker the positive ‘‘capillary charge,’’ denoted in Fig. 10, for the central particle we have $\varphi_A = (5/6)\pi + \theta - \varphi_H$. In addition, for particle 2 we have $\varphi_B = \pi - \psi + \varphi_H$, where the angle ψ is also shown in Fig. 10. From triangle $OO_2'P$ we obtain $\psi = \pi/2 - (\pi/3 - \theta)$. As a result, we get $\varphi_B = \pi - \pi/6 - \theta + \varphi_H$.

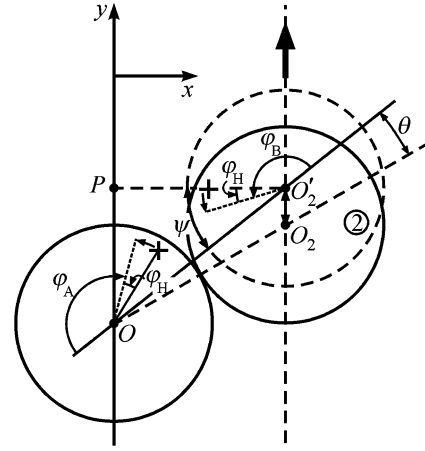


Fig. 10. Calculation of the capillary interaction between the central particle and particle 2 in Fig. 9. From the triangle $OO_2'P$ one sees that $\psi + 60^\circ - \theta = 90^\circ$. The other notations and details are explained in the text.

Consequently, $\varphi_B - \varphi_A = 2\theta - 2\varphi_H$. Substituting the latter value in Eq. (6.8), we get

$$W_2 = \pi\sigma H^2[2S_1 - G_1 \cos(6\varphi_H - 6\theta)]. \quad (6.12)$$

In a similar way, it can be proved that $W_3 = W_2$. Hence, in view of Eqs. (6.11) and (6.12), Eq. (6.7) acquires the form

$$U = 2\pi\sigma H^2[6S_1 - G_1 \cos(6\varphi_H) - 2G_1 \cos(6\varphi_H - 6\theta)]. \quad (6.13)$$

Next, to determine φ_H , we substitute Eq. (6.13) into Eq. (6.10). In this way, using the approximation $\sin(x) \approx x$ (for $x \ll 1$), we obtain

$$\varphi_H = \frac{2}{3}\theta = \frac{1}{2}\varphi_S, \quad (6.14)$$

where at the last step we have employed Eq. (6.6). The substitution of Eqs. (6.6) and (6.14) into Eq. (6.13) yields

$$U = 2\pi\sigma H^2[6S_1 - G_1 \cos(3\varphi_S) - 2G_1 \cos((3/2)\varphi_S)]. \quad (6.15)$$

Equation (6.15) gives the explicit dependence of U on φ_S , which, after a substitution in Eq. (6.3), finally leads to an expression for the surface shear elasticity:

$$E_S = 18\sqrt{3}\pi G_1 \sigma (H/L_1)^2. \quad (6.16)$$

In general, we have $L_1 \geq 2r_c$, because the electrostatic repulsion between the particles across the nonaqueous phase could keep them separated at a certain distance apart [37,38]. Thus, $G_1 = G(L_1)$ has to be calculated from Eqs. (3.3), (3.19), and (4.6). If such repulsion is missing, and the particles are in close contact, then $L_1 \rightarrow 2r_c$, $\tau_Y \rightarrow 0$, and Eq. (4.6) gives a finite limiting value for G_1 , which has been determined by us numerically:

$$G(L_1 = 2r_c) = 2.60816\dots \quad (6.17)$$

Substituting the latter value for G_1 into Eq. (6.16), we get the value of the shear elasticity at close contact between the

particles:

$$E_S = 255.46\sigma(H/2r_c)^2. \quad (6.18)$$

For example, substituting $\sigma = 50$ mN/m and $H/(2r_c) = 0.1$, from Eq. (6.18) we obtain $E_S = 127.7$ mN/m, which is a considerable value. Such monolayer should behave as a 2D elastic solid, rather than a 2D fluid. (For a fluid, $E_S = 0$ by definition.)

7. Summary and conclusions

A colloidal particle adsorbed at a fluid interface could have an undulated, or irregular, contact line when the particle shape is nonspherical, angular, or irregular in the presence of surface roughness, chemical inhomogeneity, etc. The contact-line undulations produce distortions in the surrounding liquid interface, whose overlap engenders capillary interaction between two adsorbed particles (Fig. 1b). The convex and concave local deviations of the meniscus shape from planarity can be theoretically treated as positive and negative capillary charges, which form capillary multipoles. Correspondingly, the meniscus shape can be expressed as a multipole expansion, Eq. (1.6). In general, this expansion involves multipoles of various orders. For this reason, it is important to have at our disposal equations describing the interaction between different modes. Until now, theoretical expressions have been derived only for the charge–charge [18,19] and quadrupole–quadrupole [20,21] interaction energy. As a generalization of previous studies, here, we derive expressions for the interaction between two capillary multipoles of arbitrary order; see Eqs. (4.4)–(4.6). Simpler asymptotic expressions for the interaction energy at not-too-short interparticle distances are also derived; see Eqs. (4.12) and (5.22).

Numerical results are presented for the energy of interaction between two capillary hexapoles as a function of the interparticle distance, L , and phase angle, $\Delta\varphi$, see Fig. 7. Depending on $\Delta\varphi$, the interaction could be either monotonic attraction, or monotonic repulsion, or it is attraction at long distances but repulsion at short distances. The capillary interaction energy scales as $\pi\sigma H^2$ (σ —interfacial tension, H —undulation amplitude). Typically, for $H \geq 5$ nm, this energy is much greater than the thermal energy kT . For this reason, the forces between capillary multipoles certainly influence many phenomena with particles, particle monolayers and particle arrays at fluid interfaces, although experimentally, these effects are still insufficiently explored.

Based on the results for the interaction energy, one can predict also the rheological behavior of adsorption monolayers from capillary multipoles. As an illustration, in Section 6 we derived an expression for the surface shear elasticity, E_S , of a monolayer from capillary hexapoles, Eq. (6.16). Owing to the pronounced angular dependence of the interaction energy, the adsorption monolayer of capillary multipoles exhibits a considerable shear elasticity, and should behave as a 2D elastic solid, rather than 2D fluid.

The results of this paper could be helpful for the understanding of some phenomena related to aggregation and ordering of particles adsorbed at a fluid interface, and for the interpretation of the rheological behavior of monolayers from nonspherical particles. Related research fields are the particle-stabilized (Pickering) emulsions and the two-dimensional self-assembly of microscopic particles.

Acknowledgments

This work was supported by the program “Cooperation and Networking for Excellence” (CONEX), financed by the Austrian Ministry of Education, Science, and Culture. The authors are grateful to Mariana Paraskova for her help in figure preparation.

Appendix A. The coefficients $A(n, m, \tau)$ and $B(n, m, \tau)$

Here, our aim is to determine the coefficients $A(n, m, \tau)$ and $B(n, m, \tau)$, i.e., to calculate the integrals in Eqs. (3.15) and (3.16). For this purpose, let us first consider the auxiliary integral

$$I(n, m, \alpha) \equiv \frac{1}{2\pi i} \oint_{|z|=1} z^{n-1} \frac{(\alpha z - 1)^m}{(\alpha - z)^m} dz = 0, \quad (A.1)$$

where $m \geq 0$; $n \geq 1$; $\alpha = \exp(\tau\gamma) > 1$; i is the imaginary unit; z is a complex variable; and the integration is carried out over the unit circumference, $|z| = 1$, in the complex plane—see Fig. 11. The integral in Eq. (A.1) is equal to zero, because the integrand has no singular points inside the area encircled by the contour of integration. Next, let us substitute

$$z = \exp(i\omega) \quad \text{at } |z| = 1. \quad (A.2)$$

With the help of Eq. (A.2) we obtain

$$\begin{aligned} \frac{\alpha z - 1}{\alpha - z} &= \frac{\alpha \cos \omega - 1 + i\alpha \sin \omega}{\alpha - \cos \omega - i \sin \omega} \\ &= \frac{(\alpha^2 + 1) \cos \omega - 2\alpha}{\alpha^2 - 2\alpha \cos \omega + 1} + i \frac{(\alpha^2 - 1) \sin \omega}{\alpha^2 - 2\alpha \cos \omega + 1}. \end{aligned} \quad (A.3)$$

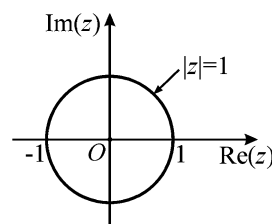


Fig. 11. The integration in Eq. (A.1) is carried out over the unit circumference, $|z| = 1$, in the complex plane.

Having in mind the definition of α , and Eqs. (3.10) and (3.11), we bring Eq. (A.3) into the following simpler form:

$$\frac{\alpha z - 1}{\alpha - z} = \exp(i\varphi). \quad (\text{A.4})$$

Further, we substitute Eqs. (A.2) and (A.4) into Eq. (A.1), and derive

$$\begin{aligned} I(n, m, \alpha) &= \frac{1}{2\pi} \int_{-\pi}^{\pi} \exp[i(n\omega + m\varphi)] d\omega \\ &= \frac{1}{2\pi} \int_{-\pi}^{\pi} \cos(n\omega + m\varphi) d\omega. \end{aligned} \quad (\text{A.5})$$

Comparing the definitions, Eqs. (3.15) and (3.16), with Eq. (A.5), we obtain $2I(n, m, \alpha) = A(n, m, \tau_Y) - B(n, m, \tau_Y)$. However, Eq. (A.1) shows that $I(n, m, \alpha) = 0$. Hence,

$$A(n, m, \tau_Y) = B(n, m, \tau_Y) \quad (n \geq 1). \quad (\text{A.6})$$

See also Eq. (3.17) in the main text. Next, let us consider the integral

$$I(n, -m, \alpha) \equiv \frac{1}{2\pi i} \oint_{|z|=1} z^{n-1} \frac{(\alpha - z)^m}{(\alpha z - 1)^m} dz, \quad (\text{A.7})$$

where $m \geq 1$ and $n \geq 1$. In Eq. (A.7), the integrand has a pole of m th order at $z = 1/\alpha$, inside the unit circle $|z| \leq 1$. Then, with the help of the residuum theorem, we obtain

$$\begin{aligned} I(n, -m, \alpha) &= \text{Res}_{z=1/\alpha} \left\{ z^{n-1} \frac{(\alpha - z)^m}{(\alpha z - 1)^m} \right\} \\ &= \frac{1}{(m-1)! \alpha^m} \left. \frac{d^{m-1}}{dz^{m-1}} [z^{n-1} (\alpha - z)^m] \right|_{z=1/\alpha}. \end{aligned} \quad (\text{A.8})$$

Next, we replace m with $-m$ in Eq. (A.5) and compare the result with Eqs. (3.15), (3.16), and (A.6). Thus we find

$$I(n, -m, \alpha) = A(n, m, \tau_Y). \quad (\text{A.9})$$

The combination of Eqs. (A.8) and (A.9) yields Eq. (3.17) in the main text. Further, in Eq. (A.8) we introduce the variables $\beta = \alpha^{-1}$ and $t = \beta z$. Using the binomial expansion, we derive

$$\begin{aligned} A(n, m, \tau_Y) &= \frac{\beta^{m-n}}{(m-1)!} \\ &\times \frac{d^{m-1}}{dt^{m-1}} \sum_{k=0}^m (-1)^{m-k} \binom{m}{k} t^{m-k+n-1} \Big|_{t=\beta^2}. \end{aligned} \quad (\text{A.10})$$

Finally, we carry out the differentiation in Eq. (A.10), and obtain Eq. (3.19).

Appendix B. Asymptotics of G , S_A , and S_B

From Eq. (3.19) it follows that

$$\begin{aligned} \beta^n A(n, m, \tau_Y) &= m \sum_{k=0}^{\min(m,n)} \frac{(-1)^{m-k} (m+n-k-1)!}{(m-k)!(n-k)!k!} \beta^{m+2n-2k}. \end{aligned} \quad (\text{B.1})$$

For $n \leq m$, the minimal possible power of β , in the right-hand side of Eq. (B.1), corresponds to the maximal value of k , which is $k = n$. Then, for $\beta \ll 1$, the leading term in Eq. (B.1) is

$$\beta^n A(n, m, \beta) = (-1)^{m-n} \frac{m!}{(m-n)!n!} \beta^m + \dots \quad (n \leq m). \quad (\text{B.2})$$

For $n > m$, the maximal value of k is $k = m$, and thus the minimal possible power of β in Eq. (B.1) is $\beta^{2n-m} \ll \beta^m$. Hence, the leading term in the asymptotics of Eq. (B.1) is that given by Eq. (B.2).

For $\beta_Y \equiv \exp(-\tau_Y) \approx r_Y/L \ll 1$, the general term in the sum in Eq. (4.6) can be presented in the form

$$\begin{aligned} \frac{n A(n, m_A, \tau_A) A(n, m_B, \tau_B)}{\sinh[n(\tau_A + \tau_B)]} \\ \approx 2n \beta_A^n \beta_B^n A(n, m_A, \beta_A) A(n, m_B, \beta_B). \end{aligned} \quad (\text{B.3})$$

The substitution of Eqs. (B.2) and (B.3) into Eq. (4.6) leads to the asymptotic expression for G , Eq. (4.10).

What concerns the asymptotics of S_A and S_B for $L \rightarrow \infty$, we could not find a general analytical derivation, like that for G above. For this reason, we expanded Eq. (4.5) in series for $\beta_Y \ll 1$ by means of a computer program for mathematical transformations, “Mathematica 3.0” (Wolfram Research Inc.). In this way, we established the validity of Eqs. (4.8) and (4.9) for m_A and m_B taking any of the values 1, 2, 3, 4, and 5.

References

- [1] M. Yamaki, J. Higo, K. Nagayama, *Langmuir* 11 (1995) 2975–2978.
- [2] N. Bowden, A. Terfort, J. Carbeck, G.M. Whitesides, *Science* 276 (1997) 233–235.
- [3] N. Bowden, I.S. Choi, B.A. Grzybowski, G.M. Whitesides, *J. Am. Chem. Soc.* 121 (1999) 5373–5391.
- [4] D.B. Wolfe, A. Snead, C. Mao, N.B. Bowden, G.M. Whitesides, *Langmuir* 19 (2003) 2206–2214.
- [5] P.A. Kralchevsky, N.D. Denkov, *Curr. Opin. Colloid Interface Sci.* 6 (2001) 383–401.
- [6] J. Lucassen, *Colloids Surf.* 65 (1992) 131–137.
- [7] P.A. Kralchevsky, K. Nagayama, *Particles at Fluid Interfaces and Membranes*, Elsevier, Amsterdam, 2001, chs. 8 and 12.
- [8] S. Arditty, V. Schmitt, J. Giermanska-Kahn, F. Leal-Calderon, *J. Colloid Interface Sci.* 275 (2004) 659–664.
- [9] J.L. Keddie, *Mater. Sci. Eng.* 21 (1997) 101–107.
- [10] L. Shmuylovich, A.Q. Shen, H.A. Stone, *Langmuir* 18 (2002) 3441–3445.
- [11] O.D. Velev, K. Furusawa, K. Nagayama, *Langmuir* 12 (1996) 2374–2384.
- [12] A.D. Dinsmore, M.F. Hsu, M.G. Nikolaidis, M. Marquez, A.R. Bausch, D.A. Weitz, *Science* 298 (2002) 1006–1009.
- [13] C. Lopez, *Adv. Mater.* 15 (2003) 1679–1704.
- [14] V.N. Truskett, K.J. Stebe, *Langmuir* 19 (2003) 8271–8279.

- [15] F.Q. Fan, K.J. Stebe, *Langmuir* 20 (2004) 3062–3067.
- [16] N. Rana, S.T. Yau, *Nanotechnology* 15 (2004) 275–278.
- [17] B.V. Derjaguin, V.M. Starov, *Colloid J. USSR* 39 (1977) 383–386.
- [18] D.Y.C. Chan, J.D. Henry, L.R. White, *J. Colloid Interface Sci.* 79 (1981) 410–418.
- [19] V.N. Paunov, P.A. Kralchevsky, N.D. Denkov, K. Nagayama, *J. Colloid Interface Sci.* 157 (1993) 100–112.
- [20] D. Stamou, C. Duschl, D. Johannsmann, *Phys. Rev. E* 62 (2000) 5263–5272.
- [21] P.A. Kralchevsky, N.D. Denkov, K.D. Danov, *Langmuir* 17 (2001) 7694–7705.
- [22] P.A. Kralchevsky, K. Nagayama, *Adv. Colloid Interface Sci.* 85 (2000) 145–192.
- [23] M.G. Nikolaidis, A.R. Bausch, M.F. Hsu, A.D. Dinsmore, M.P. Brenner, C. Gay, D.A. Weitz, *Nature* 420 (2002) 299–301.
- [24] D. Langevin, *Chem. Phys. Phys. Chem.* 4 (2003) 1057–1058.
- [25] K.D. Danov, P.A. Kralchevsky, M.P. Boneva, *Langmuir* 20 (2004) 6139–6151.
- [26] J.-B. Fournier, P. Galatola, *Phys. Rev. E* 65 (2002) 031601.
- [27] A.B.D. Brown, C.G. Smith, A.R. Rennie, *Phys. Rev. E* 62 (2000) 951–960.
- [28] J.C. Loudet, A.M. Alsayed, J. Zhang, A.G. Yodh, *Phys. Rev. Lett.* 94 (2005) 018301.
- [29] T. Tlusty, S.A. Safran, *Science* 290 (2000) 1328–1331.
- [30] U.S. Schwarz, S.A. Safran, *Phys. Rev. Lett.* 88 (2002) 048102.
- [31] E. Janke, F. Emde, F. Lösch, *Tables of Higher Functions*, McGraw–Hill, New York, 1960.
- [32] M. Abramowitz, I.A. Stegun, *Handbook of Mathematical Functions*, Dover, New York, 1965.
- [33] A.J. McConnell, *Application of Tensor Analysis*, Dover, New York, 1957.
- [34] G.A. Korn, T.M. Korn, *Mathematical Handbook*, McGraw–Hill, New York, 1968.
- [35] P.A. Kralchevsky, V.N. Paunov, N.D. Denkov, I.B. Ivanov, K. Nagayama, *J. Colloid Interface Sci.* 155 (1993) 420–437.
- [36] L.D. Landau, E.M. Lifshitz, *Theory of Elasticity*, Pergamon, Oxford, 1970.
- [37] R. Aveyard, B.P. Binks, J.H. Clint, P.D.I. Fletcher, T.S. Horozov, B. Neumann, V.N. Paunov, J. Annesley, S.W. Botchway, D. Nees, A.W. Parker, A.D. Ward, A. Burgess, *Phys. Rev. Lett.* 88 (2002) 246102.
- [38] T.S. Horozov, R. Aveyard, J.H. Clint, B.P. Binks, *Langmuir* 19 (2003) 2822–2829.